INORGANIC CHEMISTRY
FRONTIERS

RESEARCH ARTICLE

View Article Online
View Journal | View Issue

Cite this: *Inorg. Chem. Front.*, 2020, **7**, 140

Solvatochromic dual luminescence of Eu–Au dyads decorated with chromophore phosphines†

Andrey Belyaev, [a] Sofia O. Slavova, [b] Igor V. Solovyev,[c] Vladimir V. Sizov, [c] Janne Jänis, [a] Elena V. Grachova *[c] and Igor O. Koshevoy *[a]

Phosphine ligands, containing chromophore substituents –π-spacer–NPh_2 (π-spacer = biphenyl, **L1**; naphthalene-ethynylphenyl, **L2**; and ethynyl-(phenylethynyl)anthracene, **L3**), were used to generate the corresponding gold(I) alkynyl complexes **Au1–Au3** (alkynyl = ethynylphenyl-2,2′-bipyridine, epbpy). These compounds demonstrate intense fluorescence, which originates from the bipolar donor–π-acceptor systems of coordinated phosphines with negligible contribution from the epbpy fragment. Due to the charge transfer characteristic of the excited state, **Au1–Au3** reveal significant emission solvatochromism (particularly discernible for **Au2**, 428 nm in cyclohexane → 580 nm in acetonitrile). The bipyridine moiety of **Au1–Au3** was utilized for binding these metalloligands to the {$Eu(tta)_3$} red emitter (tta = 3-thenoyltrifluoroacetonate) to give a family of novel dyads **Au1Eu–Au3Eu**. Incomplete energy transfer from **L1–L3** to lanthanide ions, which are primarily sensitized by diketonate ligands, leads to dual luminescence. Analogous to the parent complexes **Au1–Au3**, the fluorescence component of the dyads is highly sensitive to the solvent polarity that provides great opportunities for color tuning, including white light generation.

Received 12th August 2019,
Accepted 12th October 2019

DOI: 10.1039/c9qi01015g

rsc.li/frontiers-inorganic

Introduction

The construction of tunable multicolor photoluminescent compounds and single molecule-based materials, particularly those capable of efficient white-light emission, continues to be an appealing research topic. From practical viewpoint, such species with panchromatic luminescence could significantly advance the fabrication of organic optoelectronic devices (white light emitting diodes and electrochemical cells), and they are highly desired as a gain medium for wide-spectra lasers in the development of new sensing techniques and photoswitches.[1] For example, in order to achieve white light emission, a chromophore molecule should generate two complementing bands (*e.g.* blue and orange) or produce a combination of pure red, green and blue colors. The implementation of multicolor emission from a single molecule or a single component material remains a substantial challenge for molecular design and engineering.

Recent progress achieved for panchromatic pure organic and metal–organic luminophores illustrates that multi-band single-molecular emission can be realized *via* different physical phenomena. Among them, it is possible to identify excited-state intramolecular proton transfer,[2] aggregate formation, and conformational change to induce simultaneous locally excited and charge-transfer luminescence[3] including the combination of monomer and excimer emission,[4] stimulation of dual fluorescence and phosphorescence.[5] Nevertheless, these systems often suffer from a lack of control and tuning of their optical properties. An extensively utilized alternative approach implies the binding of two or more individual emitters in one molecular entity through a spacer, thus forming dyads or multi-chromophore assemblies. The reported single-molecule assemblies of this sort represent diverse combinations of constituting components, which may comprise covalently linked organic dyes,[6] d-block chromophores connected to organic fluorophores,[7] and homo- or heteronuclear d–d,[8] d–f[9] and f–f[10] dyads and triads. In this regard, rare earth metal ions (*e.g.* Eu(III), Tb(III), Gd(III), Dy(III), and Sm(III)) distinctly stand out in the design of versatile supramolecular aggregates showing multicolor luminescence.[9a,c,e] Pure colors and very sharp emission bands, long lifetimes and large Stokes shifts of Ln(III) f → f transitions are beneficial characteristics for responsive molecular materials, *i.e.* chemosensors,[10b,11] molecular thermometers,[12] biological probes and imaging agents.[9c,13] Although the f → f transitions are parity-forbidden by the Laporte rule,[14] the excited states of lanthanides can be populated *via* the energy transfer from, *e.g.* the adjacent d-metal chromophore.[15] This concept was successfully

[a]*Department of Chemistry, University of Eastern Finland, Joensuu, 80101, Finland. E-mail: igor.koshevoy@uef.fi*
[b]*Institute of General and Inorganic Chemistry, Bulgarian Academy of Sciences, Sofia, 1113, Bulgaria*
[c]*Institute of Chemistry, St. Petersburg State University, Universitetskii pr. 26, 198504 St. Petersburg, Russia. E-mail: e.grachova@spbu.ru*
† Electronic supplementary information (ESI) available: Synthetic, other experimental and computational details. See DOI: 10.1039/c9qi01015g

used by De Cola *et al.* in 2005 who described the d–f heterometallic assembly with panchromatic emission, where the sensitization of the Eu(III) center by means of a partial energy transfer from the blue emitting cyclometalated Ir(III) fragment to the red Eu(III) emitter generates white light with a quantum yield of 7% in solution.[16] Later, the utilization of various d-chromophores (Pt(II),[17] Ir(III),[12d,18] Os(II),[19] Ru(II),[19,20] Re(I),[17b,21] *etc.*) as antennae for lanthanide energy acceptors has rapidly expanded the family of d–f dyads. Analysis of their photophysical behavior indicates that d → f excitation transfer might occur through the conjugated system or by means of the Förster and Dexter mechanisms; some back donation to the d-containing fragment cannot be excluded.

Ultimately, incomplete energy transfer from the organic chromophore to the f-center has been exploited to produce dual or multiple emissions from single molecules.[22] Different signals, originating from the f element and the fluorescent motif of these luminophores, can demonstrate distinct responses to the environmental changes that have been applied for sensing purposes.[22b,23] A delicate balance between the lanthanide emission and fluorescence in the visible region was demonstrated by Duan *et al.* in 2009 *via* rational tailoring of the Eu(III) diketonate unit to the coumarin–rhodamine 6G fluorescent moiety. The resulting dye demonstrates excitation-dependent luminescence in solution and in the film with an overall quantum yield of nearly white emission reaching 2.5%.[24] Nonetheless, during the last decade, there has been a limited number of subsequent reports on multicolor luminescence from lanthanide complexes decorated with ancillary fluorophore antenna,[25] especially those capable of dynamic emission changes.[26]

Herein, we describe a facile strategy to prepare dual luminescent compounds by incorporating the beta-diketonate Eu(III) red emissive fragment into the bipyridine-functionalized alkynyl gold(I)–phosphine complexes, which serve as fluorescent metalloligands. For this purpose, we employ phosphines containing extended π-spacers decorated with the diphenylamine donor group. Their coordination to the Au(I) ion converts the PR_3 moiety into an electron acceptor and results in a bipolar D–π-A architecture of the pendant chromophore. This feature, in turn, induces an intramolecular charge transfer in the excited state, which is highly sensitive to the polarity of the medium and provides a remarkable tunability of the emission color of the novel dyads.

Results and discussion

Synthesis and characterization

The design of the phosphine building blocks relies on the Ph_2P–π-spacer–NPh_2 configuration, where the length of the π-spacer is expected to vary the energy of the emission by influencing the photoinduced intramolecular charge transfer (ICT). This process can be conventionally activated in the bipolar phosphine ligands upon the oxidation of the phosphorus atom or its bonding to the Au(I) center.[27] For this purpose, we have prepared compounds **L1**[28]–**L3** in good yields from the bromo–π-spacer–NPh_2 (π-spacer = biphenyl,[29] naphthalene-ethynylphenyl[30]) and ethynylanthracenyl-ethynyl-diphenylaniline precursors (Scheme S1†). Metalloligands **Au1–Au3** were obtained by the depolymerisation of $[Au(epbpy)]_n$ (epbpy = 5-(4-ethynylphenyl)-2,2′-bipyridine)[31] with phosphines **L1–L3** under oxygen-free conditions, which is a common synthetic approach to alkynyl gold(I)–phosphine complexes.[5e,32] On the other hand, the binding of the $Eu(tta)_3$ (tta = 3-thenoyltrifluoroacetonate) luminescent motif to the diimine functions occurs under mild conditions[12d,25d,e] and was successfully utilized to convert gold complexes **Au1–Au3** into dyads **Au1Eu–Au3Eu**, which were isolated in moderately good yields (Scheme 1; for details, see the ESI†). Compounds **Au1–Au3** and **Au1Eu–Au3Eu** are nearly colorless (bearing **L1**), yellow (**L2**) and red (**L3**) powders which are stable in the solid state and in solution under ambient conditions, while phosphines **L1–L3** are easily oxidized in air when dissolved. Metalloligands and Au–Eu dyads are readily soluble in organic solvents such as dichloromethane, acetone, chloroform and toluene, sparingly to moderately in diethylether, acetonitrile and cyclohexane, and

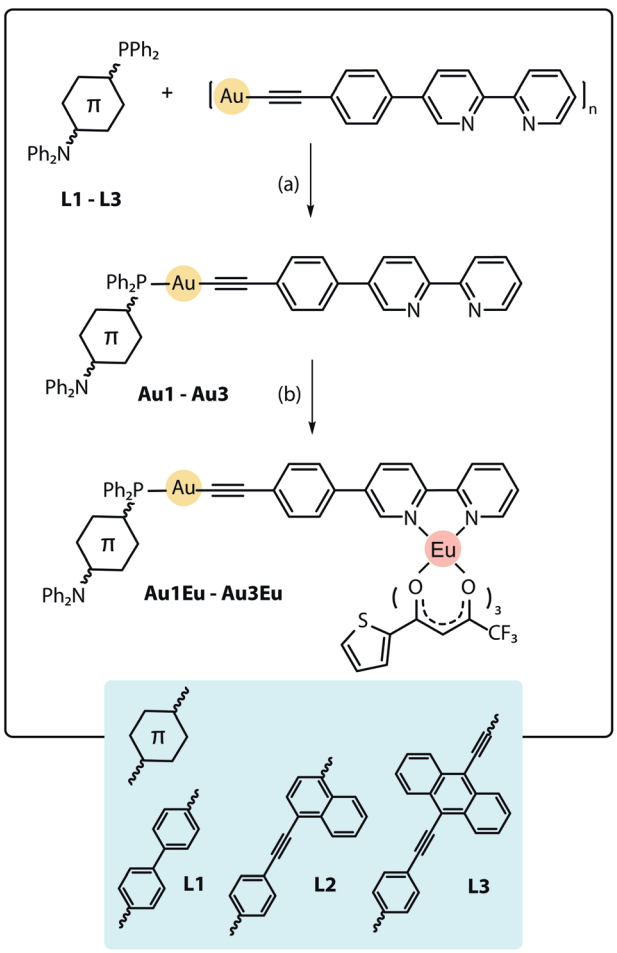

Scheme 1 Synthesis of the Au–Eu phosphine-based dyads **Au1Eu–Au3Eu**, (a) dichloromethane, 1 h, 298 K, yields 86–90%; (b) Eu $(tta)_3 \cdot 2H_2O$, dichloromethane, 1 h, 298 K, yields 72–83%.

are practically insoluble in protic media (methanol, ethanol, and water).

The $^{31}P\{^{1}H\}$ NMR spectra of **Au1–Au3** exhibit singlet peaks each in the range from 41.7 to 16.5 ppm, which are significantly shifted to the low field region compared to the free phosphines **L1–L3** (δ = −6.2 to −32.8 ppm) and therefore confirm the coordination of $-PPh_2$ groups to the Au(I) centers. Upon binding to the Eu atoms, the phosphorus NMR signals for dyads **Au1Eu–Au3Eu** virtually do not change positions with respect to the predecessor metalloligands **Au1–Au3**.

The ^{1}H NMR spectroscopic patterns for **Au1–Au3** (Fig. S1†) are completely compatible with the proposed molecular structures (Scheme 1). The corresponding spectra of the bimetallic compounds reveal a clear effect of introducing the paramagnetic Eu(III) ion into the bipyridine moiety, which is manifested by the visible broadening of the signals and a large low field shift of the resonances (δ = 14.8 and 14.4 ppm) corresponding to the diimine protons nearest to the N atoms (Fig. S2†). Furthermore, these spectra reaffirm the presence of three tta ligands around the Eu center.

Mass spectrometric measurements were performed using ESI^{+} and atmospheric pressure photoionization (APPI) techniques. For gold complexes, the dominating signals correspond to the protonated molecular ions at *m*/*z* 958.26 (**Au1**), 1032.28 (**Au2**) and 1106.29 (**Au3**) (Fig. S3).† In the case of Au–Eu successors, however, only the complicated mixtures of defragmentation species were observed.

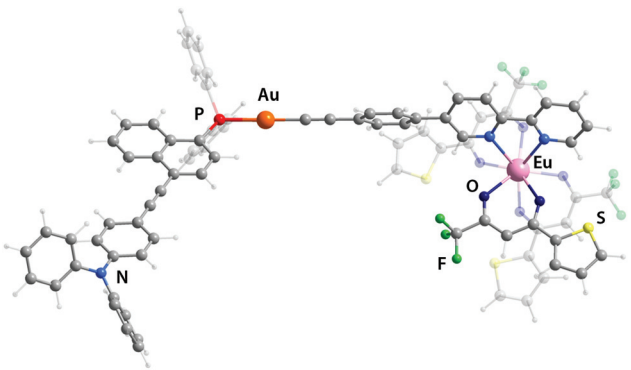

Fig. 1 Minimum energy structures of complex **Au2Eu** (the DFT LC-PBE method).

The solid state FTIR spectra of **Au1Eu–Au3Eu** demonstrate intense absorption bands at ~1600 cm^{-1}, which are attributed to the C=O stretching vibrations of the coordinated thenoyltrifluoroacetone (Fig. S4†).[25d,e] Additionally, the spectrum of **Au1Eu** exhibits a weak band at ~2114 cm^{-1} assigned to the C≡C vibration. Not surprisingly, **Au2Eu** and **Au3Eu** compounds also demonstrate distinct stretching frequencies between 2197 and 2114 cm^{-1}, which agree with the presence of several types of acetylene groups in these molecules.

Since the experimental data about the structures of these objects were not obtained, theoretical geometry optimization for all complexes has been carried out (Fig. 1 and S5,† selected bond lengths are listed in Table S1†). The LC-PBE functional with long-range correction[33] was chosen because it most accurately reproduces such geometric parameters as the lengths of the Ln–O and Ln–N bonds.[34] In general, the coordination of the $Eu(tta)_3$ fragment to the bpy motif has a negligible effect on the stereochemistry of Au(I) environment and of the remote phosphine ligand. The predicted structural parameters for the gold complexes and heterometallic dyads match well with previously reported results of the crystallographic analysis of congener compounds.[5e,18a,32b,34]

Photophysical properties

Optical behavior of metalloligands Au1–Au3 and dyads Au1Eu–Au3Eu. The UV-vis absorption and emission data for **Au1–Au3** and **Au1Eu–Au3Eu** in 1,2-dichloroethane (DCE) are summarized in Table 1 and depicted in Fig. 2. As expected, the lowest energy (LE) electronic transitions for metalloligands **Au1–Au3** are dominated by phosphines **L1–L3** (Fig. 2 and S6†). The corresponding structureless and broad absorption bands for ligands **L1–L3** demonstrate a visible red shift upon increasing the conjugated system in the order **L1** (biphenyl, 345 nm) < **L2** (naphthalene-ethynylphenyl, 385 nm) < **L3** (ethynylanthracenyl-ethynyl, 480 nm). The same trend is observed for their Au(I)-epbpy derivatives **Au1–Au3** (Fig. 2). Binding of the phosphorus donors to the gold centers induces a moderate decrease in the energy of these absorptions (λ_{abs} for **Au2** = 400 nm, for **Au3** = 495 nm) that is in line with the electron deficient properties of the coordinated P atoms and therefore enhanced the charge transfer (CT) characteristic of the LE excitation (Fig. S7†). For **Au1**, this effect is not observed because of the overlap of the CT band with characteristic higher energy

Table 1 Photophysical properties of **Au1–Au3** and **Au1Eu–Au3Eu** in solution at 298 K

	λ_{abs} [a], nm (ε, 10^{-3} M^{-1} cm^{-1})	λ_{em} [a,b], nm	$\Delta\nu$ [c], cm^{-1}	τ [d], ns	τ [e], μs	Φ_{em} [f]
Au1	330 (55.7)	460	8560	1.8	—	0.30
Au2	324 (67.9), 400 (34.6)	525	5950	1.2 (70), 3.5 (30)	—	0.31
Au3	264 (54.3), 277 (60.2), 325 (60.7), 495 (31.5)	635	4620	4.0	—	0.29
Au1Eu	271 (44.1), 339 (100.3)	460, 580, 592, 611, 654, 700	7760	2.2	280.0	0.15(0.04)
Au2Eu	280 (63.2), 337 (139.1), 404 (44.0)	525, 611	5700	1.7	434.0	0.21
Au3Eu	276 (93.6), 336 (117.8), 495 (35.8)	611, 635, 705,	4620	4.1	404.1	0.16

[a] In 1,2-dichloroethane (DCE), 1×10^{-5} M solution. [b] λ_{exc} = 360 nm. [c] The difference between the maxima of absorption and fluorescence bands. [d] Lifetime monitored at the fluorescence band. [e] Lifetime monitored at 611 nm ($^{5}D_0$–$^{7}F_2$ transition). [f] Overall quantum yield (quantum yield of the fluorescence band), relative to coumarin 102 dye (Φ = 0.76) in ethanol.

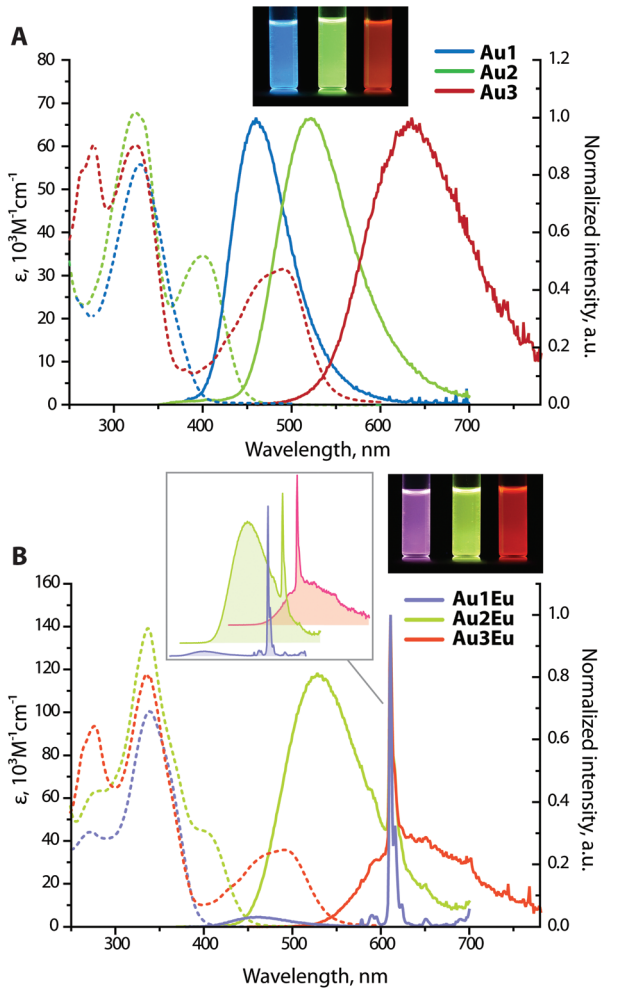

Fig. 2 UV-vis absorption (dashed lines) and normalized emission (solid lines) spectra of metalloligands **Au1–Au3** (A), and dyads **Au1Eu–Au3Eu** (B), normalized at 611 nm, the inset exhibits the stacking of the emission spectra (DCE, 298 K, λ_{exc} = 360 nm, c = 1 × 10^{-5} M); the photographs show the corresponding solutions under UV light (a broad band mercury lamp).

absorptions at *ca.* 324–330 nm with large extinction coefficients (ε = 55 700 M^{-1} cm^{-1} for **Au1**, 67 700 M^{-1} cm^{-1} for **Au2** and 60 200 M^{-1} cm^{-1} for **Au3**), attributed to the intraligand $\pi \rightarrow \pi^*$ transitions localized on the epbpy fragment.[31] This assignment is supported by quantum chemical calculations, according to which the lowest energy excitation $S_0 \rightarrow S_1$ for **Au1–Au3** occurs within the phosphine chromophores and shows a gradual growth of the wavelength from 307 to 441 nm, while the transitions $S_0 \rightarrow S_2$ (**Au1**, **Au2**) and $S_0 \rightarrow S_4$ (**Au3**) mainly involve the epbpy aromatic system (Fig. S7 and S8†). Although the predicted absorption energies are overestimated, the general tendencies correlate well with the experimental results.

Not surprisingly, optical properties of dyads **Au1Eu–Au3Eu** largely resemble those of gold-containing metalloligands (Fig. 2). The positions and intensities of the LE CT bands remain virtually unaffected upon the coordination of **Au1–Au3** to the europium(III) ion. The bands maximized around 335–340 nm, which are nearly the same for all three bimetallic complexes, reveal significantly enhanced intensities (ε are in the order of 10^5 M^{-1} cm^{-1}, see Table 1). Such substantial growth of molar absorptivities corresponds to a combination of energetically close $\pi \rightarrow \pi^*$ transitions of the phenylene-bipyridine and diketonate (tta) ligands, as suggested by the computational studies (Fig. 3, S8 and S9†), and additionally proves the presence of Eu(tta)$_3$ in the resulting dyads.

Chromophores **Au1–Au3** exhibit strong emission under 360 nm excitation in DCE solutions with similar quantum yields around 0.30, while in the solid state, the luminescence at room temperature is completely suppressed apparently due to the aggregation quenching effect. The excited state lifetimes for **Au1** (τ = 1.8 ns) and **Au3** (τ = 4.0 ns) were obtained by a monoexponential fit of the decay kinetics; for **Au2**, a biexponential treatment gave two components with τ_1 = 1.8 ns (70%) and τ_2 = 3.5 ns (30%), and an average value τ_{av} of 2.4 ns. Short lifetimes of several ns and insensitivity of the emission intensity to molecular oxygen indicate prompt fluorescence. The broad and structureless emission profiles feature a steady increase in the peak wavelength **Au1** (460 nm) < **Au2** (525 nm) < **Au3** (635 nm). Furthermore, large Stokes shifts for **Au1–Au3**, found in the range of 4620–8560 cm^{-1}, are typical of the D–π-A architectures and confirm the intramolecular charge transfer characteristic of the lowest excited state. In the case of **Au1**, the emission energy is comparable to those of the (Ph_2N-biphenyl-)$_3$P → E congeners (E = O, 448 nm; S, 450 nm; Se, 450 nm; AuC_6F_5, 457 nm in dichloromethane).[27d] With respect to the phosphonium derivatives of ligands **L1** and **L2**[30] containing stronger electron accepting cationic motifs, the emission and absorption bands of complexes **Au1** and **Au2** are found at considerably higher energies. The quantum efficiency for **Au1** (Φ_{em} = 0.30 in DCE) is substantially lower than those for its oxide analogues (0.8 in ethyl acetate for **L1**=O and 0.95 in CH_2Cl_2 for (Ph_2N-biphenyl-)$_3$P=O).[27b,d] One possible non-radiative process might be a partial population of the triplet state T_1 *via* relatively slow intersystem crossing ($S_1 \rightarrow T_1$) due to a heavy atom effect induced by a gold ion.[5e,35] The absence of phosphorescence under ambient conditions can be explained by weak spin–orbit coupling in the excited state, insufficient for promoting the $T_1 \rightarrow S_0$ radiative relaxation.

Intense phosphine-localized fluorescence of metalloligands **Au1–Au3**, which is virtually independent on the bipyridine function, is anticipated to achieve panchromatic emission upon the incorporation of the Eu(III) ion, known for its intense red luminescence. As shown in Fig. 2B, dyad **Au1Eu** exhibits two emission components. The minor HE signal centered at 460 nm matches the fluorescence band of the parent complex **Au1**, and the major set of LE peaks with maxima at 580, 592, 611, 654, and 700 nm correspond to the characteristic intra-configurational $^5D_0 \rightarrow {}^7F_n$ (n = 0–4) electronic 4f–4f transitions of the Eu(III) ion; the hypersensitive transition $^5D_0 \rightarrow {}^7F_2$ dominates over other bands. The ratio of the integral intensities for $^5D_0 \rightarrow {}^7F_2$ and $^5D_0 \rightarrow {}^7F_1$ transition (I_2/I_1) equals 12 that indicates the low symmetry of the Eu(III) local environment. The

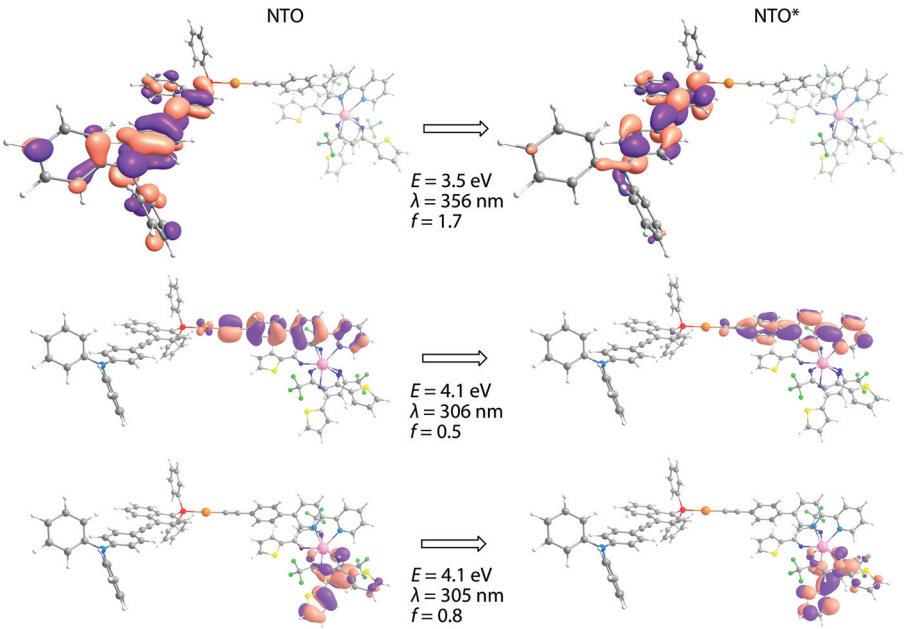

Fig. 3 Natural transition orbitals involved in the lowest energy singlet electronic excitation for complex **Au2Eu**.

overall quantum efficiency for **Au1Eu** amounts to 0.15, where fluorescence contributes only 0.04 and the rest 0.11 of the intensity appear from the lanthanide. An appreciable decrease in the singlet HE emission for **Au1Eu** compared to the parent **Au1** (Φ_{em} = 0.30) suggests the partial energy transfer from the metalloligand to the Eu(III) center.

This process is supported by the TDDFT calculated energy diagram (Fig. 4 and S8†). The singlet levels of the tta, epbpy (32 894 cm^{-1}) and phosphine **L1** (32 467 cm^{-1}) components in **Au1Eu** have very close energies and therefore are expected to be simultaneously populated upon photoexcitation and thermal equilibration. The lowest triplet state of the dyad is localized on the diketonate ligand (~20 500 cm^{-1}) meaning that the ET is also possible from the higher lying triplet levels of epbpy (~22 500 cm^{-1}) and **L1** (~23 700 cm^{-1}) to the $^5D_0$ state of Eu(III) (~17 500 cm^{-1}).[36] Direct sensitization of the Eu(III) ion by means of the epbpy ligand is confirmed by the emergence of the lanthanide emission upon treating **Au1–Au3** fluorophores with $Eu(NO_3)_3$ (Fig. S10).†

The luminescence spectra of **Au2Eu** and **Au3Eu** exhibit two-component profiles dominated by fluorescence bands at 525 and 635 nm, respectively, accompanied by the sharp emission peak of the europium ion positioned at 611 nm. The predicted lowest energy singlet and triplet excited states for the gold complexes and the dyads correspond to phosphine ligands (Fig. 4 and S8†) that prevent the ET from **L2** and **L3** to the Eu-coordinated bpy and tta moieties. The total quantum yields for **Au2Eu** (Φ_{em} = 0.21) and **Au3Eu** (Φ_{em} = 0.16) also decrease with respect to their gold precursors **Au2** and **Au3**. The lower lying charge transfer triplets (~18 000 cm^{-1} for **Au2Eu** and ~10 530 cm^{-1} for **Au3Eu**) might allow back transfer of the excitation energy from $^5D_0$(Eu(III)) to dark ^{3}CT(**L2**/**L3**) states that

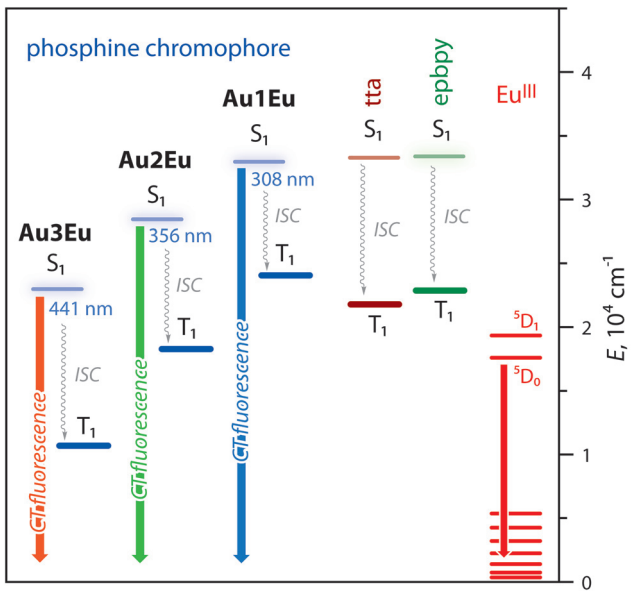

Fig. 4 Excited state diagrams for complexes **Au1Eu–Au3Eu** predicted by TDDFT analysis. The energies of tta and epbpy ligands are virtually the same for all dyads (see the complete diagram in Fig. S8†).

presumably accounts for the decrease in the intensity of both lanthanide and phosphine-centered singlet emissions.

The emission lifetimes for **Au1Eu–Au3Eu**, determined by the monoexponential fit of the fluorescence decays, correlate with the corresponding values for metalloligands **Au1–Au3**. The luminescence for **Au1Eu–Au3Eu** monitored at 611 nm produced rather long lifetimes of 280.0, 434.0 and 404.1 μs,

respectively, which are typical of the radiative relaxation of the Eu(III) ion.[37]

Solvatochromic behavior. In order to probe the sensitivity of the donor–π-acceptor systems of the phosphine–Au(I) fragments to the properties of the environment and to manipulate the dual emission of the dyads, we studied the photophysical behavior of **Au1–Au3** and of their bimetallic derivatives **Au1Eu–Au3Eu** in solvents with different polarities (cyclohexane (CHX), toluene, dichloromethane (DCM), chloroform, diethyl ether, tetrahydrofuran (THF), acetone, and acetonitrile (MeCN)). The relevant absorption and emission spectra are given in Fig. 5, 6 and S11–S15† and the data are listed in Tables 2 and S2.†

Increasing the solvent polarity from cyclohexane to acetonitrile leads to an insignificant, but detectable, hypsochromic shift for 7–13 nm (296–820 cm^{-1}) of the CT band in the absorption spectra of metalloligands **Au1–Au3** (Fig. S11†).

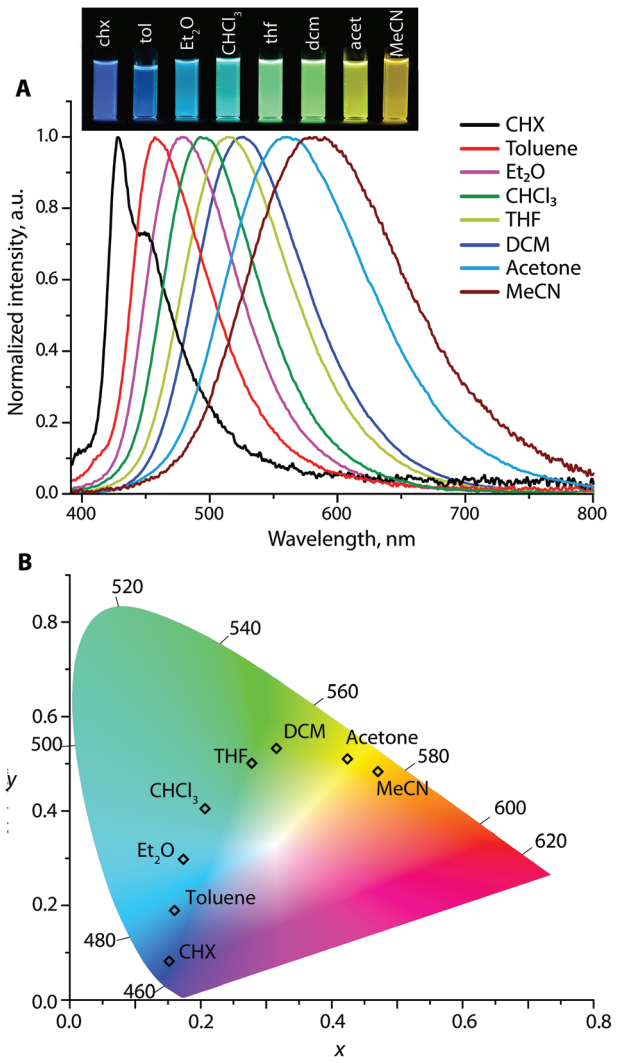

Fig. 5 (A) The emission spectra (λ_{exc} = 365 nm, normalized on the fluorescence band) and (B) CIE 1931 coordinates of **Au2** in different solvents (the photograph shows the corresponding solutions under a broad band mercury lamp).

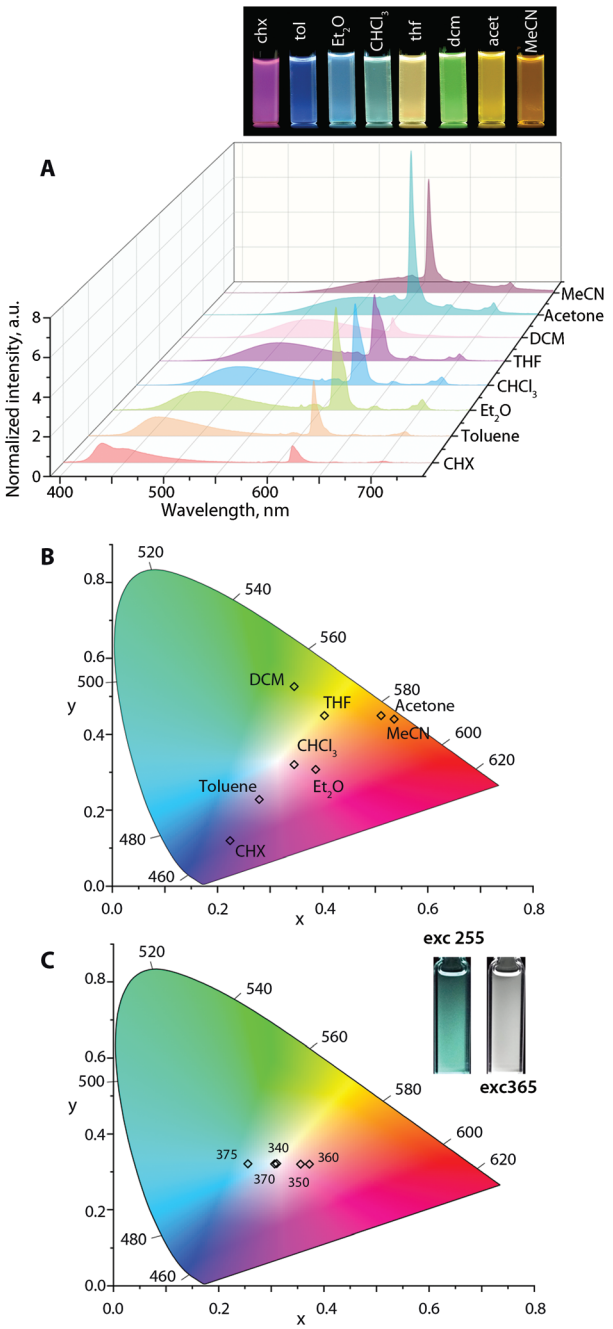

Fig. 6 (A) The emission spectra (λ_{exc} = 365 nm, normalized on the fluorescence band; the photograph shows the corresponding solutions under a broad band mercury lamp). (B) CIE 1931 coordinates for **Au2Eu** in different solvents (λ_{exc} = 365 nm). (C) CIE 1931 coordinates for **Au2Eu** in chloroform at different excitation wavelengths, and the inset shows the visual appearance of the solutions under 255 and 365 nm excitation.

Small negative solvatochromism can be tentatively explained by the solvent–molecule interaction that leads to a certain stabilization of the ground state S_0 in a medium of higher polarity. Analysis of the composition of NTOs involved in the LE electronic transitions supports these observations. Considering complex **Au3** as an example, one can see that

Table 2 Photophysical characteristics of **Au1Eu–Au3Eu** in different solvents at 298 K

	CHX	Toluene	Et_2O	$CHCl_3$	THF	DCM	Acetone	MeCN
	Au1Eu							
λ_{abs} [a]	342	339	337	336	339	338	334	335
λ_{em} [a,b]	403, 423	425	435	445	450	460	475	490
CIE[c]	0.34, 0.13	0.56, 0.26	0.27, 0.12	0.30, 0.16	0.29, 0.18	0.52, 0.28	0.35, 0.28	0.52, 0.33
	Au2Eu							
λ_{abs} [a]	334, 405	336, 402	330, 393	321, 402	334, 396	322, 401	393	328, 392
λ_{em} [a,b]	428, 450	460	480	495	515	525	560	580
CIE[c]	0.22, 0.11	0.28, 0.23	0.39, 0.31	0.35, 0.32	0.40, 0.45	0.34, 0.52	0.51, 0.45	0.53, 0.44
	Au3Eu							
λ_{abs} [a]	336, 494	337, 498	333, 486	334, 492	336, 488	336, 494	332, 484	333, 483
λ_{em} [a,b]	520, 555	550	572	590	—[d]	630	—[d]	—[d]
CIE[c]	0.37, 0.58	0.46, 0.53	0.58, 0.41	0.59, 0.39	0.64, 0.36	0.61, 0.38	0.66, 0.33	0.67, 0.33

[a] Measured at 0.15 O.D. at the excitation wavelength. [b] Fluorescence band, λ_{exc} = 365 nm. [c] (x, y) coordinates calculated from emission spectra. [d] Only Eu-emission was observed.

both the NTO and NTO* orbitals are predominantly localized on diphenylaniline and diethynyl–anthracene fragments (Fig. S7†). For the solvent with the lowest polarity (cyclohexane), their contributions to the NTO are 22% and 76%. This ratio changes with increasing the solvent polarity, reaching 30% : 69% for acetonitrile. Unlike the NTO orbital, NTO* appears to be unaffected by the properties of the solvent.

In nonpolar cyclohexane, the emission spectra of the **Au1–Au3** appear as roughly structured bands with vibronic progressions of *ca.* 1140–1210 cm^{-1}, which are attributed to the relaxation of locally excited (LE) states (Fig. 5, S12 and S13†). For example, the signal of **Au1** with maxima at 403 (0 → 0 transition) and 423 nm ($\Delta\nu$ = 1170 cm^{-1}) correlates with the fluorescence profile of *N*,*N*-diphenyl-biphenyl amine[38] but is red-shifted for ~50 nm due to the presence of the electron-accepting Ph_2P → Au group. In more polar solvents, the emission bands for **Au1–Au3** become broad and featureless, and gradually move to a low energy region due to the prevailing charge transfer characteristic of the radiative relaxation. For instance, **Au2** in cyclohexane produces nearly pure deep blue emission (λ_{em} = 428 and 450 nm) with the Commission Internationale de l'Eclairage (CIE) coordinates (0.15, 0.08), green in dichloromethane λ_{em} = 525 nm (CIE 0.31, 0.53), and orange λ_{em} = 580 nm (0.47, 0.48) in acetonitrile, revealing a prominent red shift of 152 nm (4719 cm^{-1}) (Fig. 5). However, the diversity of colors for **Au1** and **Au3** is less pronounced; their CIE coordinates vary from violet-blue to green (0.15, 0.02) → (0.20, 0.34) for **Au1**, and from green-yellow to red (0.33, 0.61) → (0.48, 0.40) for **Au3** (Fig. S12 and S13†). The Stokes shifts for **Au1–Au3** vary from 1177–5126 cm^{-1} in cyclohexane to larger values of 5689–10 173 cm^{-1} in polar acetonitrile that points to a significant stabilization of the ICT excited state.

The solvent-dependent behavior of **Au1–Au3** was examined using the Lippert–Mataga approach (see Fig. S14† and the description of the procedure in the Experimental section),[39] which treats the Stokes shift of a CT fluorophore as a linear function of the solvent polarity. The slopes of these plots for metalloligands **Au1–Au3** provide the changes in the dipole moments ($\Delta\mu = \mu_{es} - \mu_{gs}$), which occur upon excitation, and amount to *ca.* 24, 33 and 37 D, respectively; these values are typical of neutral donor–acceptor molecules.

The absorption spectra of dyads **Au1Eu–Au3Eu** slightly differ from those of metalloligands **Au1–Au3**. The main intense peak centered at ~330 nm is attributed to the π → π* tta-centered transitions, which are almost insensitive to the solvent polarity, while the CT bands follow the same trend as for **Au1–Au3**, and show a small hypsochromic shift of *ca.* 11–13 nm upon polarity increase (Fig. S11†).

Analogous to **Au1–Au3**, the emission profiles for **Au1Eu–Au3Eu** (Fig. 6, S15 and S16†) exhibit a bathochromic shift in the broad fluorescence band in polar media. In contrast, the position of sharp $^5D_0 \rightarrow {}^7F_n$ (n = 0–4) Eu(III) transitions maximized at 611 nm remains unaffected (although the intensities vary) that results in a large diversity of the luminescence colors according to the calculated CIE coordinates. For instance, at the excitation wavelength of 365 nm, **Au2Eu** in $CHCl_3$ and Et_2O exhibits nearly white emission with coordinates (0.35, 0.32) and (0.39, 0.31). In more polar MeCN and acetone solutions, the color of all dyads appears in the reddish-orange zone of the chromaticity diagram (for **Au2Eu** CIE 0.51, 0.45 and 0.53, 0.44, respectively; Fig. 6) due to a significant quenching of the fluorescence band and the domination of the lanthanide luminescence. The emissions of **Au1Eu** and **Au3Eu** dyads correspond to different regions of the color space. The color of **Au3Eu** steadily changes from green-yellow (cyclohexane) to red (acetonitrile), but **Au1Eu** shows irregular alterations from magenta (diethyl ether) to orange (acetonitrile) and red (toluene) (Fig. S15 and S16).† In addition to the solvatochromic effect, the excitation energy distinctly affects the intensity ratio of the fluorescence and lanthanide emission bands, as illustrated by the response of the **Au2Eu** complex in $CHCl_3$ solution to the excitation wavelengths, ranging from 280 nm to 400 nm (Fig. S17†). Notably, using the radiation from 320 to 375 nm allowed influencing primarily the x coordinate (0.26, 0.32 → 0.37, 0.32), and, particularly with 340 and 370 nm excitation, to achieve the CIE values (0.31, 0.32), which

are close to pure white color. When the excitation shifted to lower energy (390–400 nm), only the fluorescence band was observed for **Au2Eu**, which confirms the absence of energy transfer from the intraphosphine ^{1}CT state to the europium ion.

Conclusions

The chromophore-containing phosphines **L1–L3**, based on diphenylamine-functionalized conjugated systems, produce highly fluorescent species **Au1–Au3** upon coordination to the gold(I)-alkynyl fragments. Their photophysical properties are determined by the intraligand (**L1–L3**) electronic transitions that are confirmed by the DFT computational analysis. Due to the intrinsic donor–acceptor nature of the metal-bound phosphine motifs, complexes **Au1–Au3** undergo photoinduced intramolecular charge transfer, which results in pronounced luminescence solvatochromism (428 nm in cyclohexane → 580 nm in acetonitrile for **Au2**). Furthermore, the incorporation of the chelating bipyridine unit into the Au-connected alkynyl offers a facile opportunity to utilize compounds **Au1–Au3** as metalloligands. As a proof of concept, these gold(I) precursors were combined with the {Eu(tta)$_3$} moiety to give a family of dyads **Au1Eu–Au3Eu**. Efficient sensitization of the lanthanide emission by diketonates (tta) and partial excitation energy transfer from intra-phosphine ^{1}CT states, particularly suppressed for **L2** and **L3**, lead to the dual luminescence combined with fluorescence and europium-centered transitions. The dynamic features of **Au1–Au3** emission behavior, governed by the properties of the medium, are retained in bimetallic assemblies **Au1Eu–Au3Eu**. This, together with the excitation-dependent ratio of the phosphine and lanthanide emissions, offers rich opportunities for tuning the luminescence color. The described complexes represent the first examples of merging the remote charge-transfer highly solvatochromic fluorophores with red-emitting Eu centers and demonstrate a convenient approach in the design of dual emissive complexes with widely variable luminescence characteristics.

Conflicts of interest

There are no conflicts to declare.

Acknowledgements

The authors appreciate the financial support from the Academy of Finland (grant 317903, I. O. K.) and the Russian Science Foundation (grant 16-13-10064, photophysical and computational investigations, E. V. G., V. V. S., and S. O. S.). The work was carried out using the core facilities of St Petersburg State University Research Park (Centre for Magnetic Resonance, Centre for Optical and Laser Materials Research, Computer Centre).

References

1 (*a*) I. D. W. Samuel and G. A. Turnbull, *Chem. Rev.*, 2007, **107**, 1272–1295; (*b*) A. J. C. Kuehne and M. C. Gather, *Chem. Rev.*, 2016, **116**, 12823–12864; (*c*) G. M. Farinola and R. Ragni, *Chem. Soc. Rev.*, 2011, **40**, 3467–3482; (*d*) M.-S. Wang and G.-C. Guo, *Chem. Commun.*, 2016, **52**, 13194–13204; (*e*) D. Kim and S. Y. Park, *Adv. Opt. Mater.*, 2018, **6**, 1800678; (*f*) S.-C. Lee, J. Heo, H. C. Woo, J.-A. Lee, Y. H. Seo, C.-L. Lee, S. Kim and O. P. Kwon, *Chem. – Eur. J.*, 2018, **24**, 13706–13718; (*g*) D. Li, J. Wang and X. Ma, *Adv. Opt. Mater.*, 2018, **6**, 1800273.

2 (*a*) V. S. Padalkar and S. Seki, *Chem. Soc. Rev.*, 2016, **45**, 169–202; (*b*) S. Park, J. E. Kwon, S. H. Kim, J. Seo, K. Chung, S.-Y. Park, D.-J. Jang, B. M. Medina, J. Gierschner and S. Y. Park, *J. Am. Chem. Soc.*, 2009, **131**, 14043–14049; (*c*) K.-C. Tang, M.-J. Chang, T.-Y. Lin, H.-A. Pan, T.-C. Fang, K.-Y. Chen, W.-Y. Hung, Y.-H. Hsu and P.-T. Chou, *J. Am. Chem. Soc.*, 2011, **133**, 17738–17745; (*d*) B. Li, J. Lan, D. Wu and J. You, *Angew. Chem., Int. Ed.*, 2015, **54**, 14008–14012; (*e*) S. Tsuchiya, K.-I. Sakai, K. Kawano, Y. Nakane, T. Kikuchi and T. Akutagawa, *Chem. – Eur. J.*, 2018, **24**, 5868–5875; (*f*) B. Li, L. Zhou, H. Cheng, Q. Huang, J. Lan, L. Zhou and J. You, *Chem. Sci.*, 2018, **9**, 1213–1220.

3 (*a*) X.-H. Jin, C. Chen, C.-X. Ren, L.-X. Cai and J. Zhang, *Chem. Commun.*, 2014, **50**, 15878–15881; (*b*) Z. Xie, C. Chen, S. Xu, J. Li, Y. Zhang, S. Liu, J. Xu and Z. Chi, *Angew. Chem., Int. Ed.*, 2015, **54**, 7181–7184; (*c*) D. Tu, P. Leong, S. Guo, H. Yan, C. Lu and Q. Zhao, *Angew. Chem., Int. Ed.*, 2017, **56**, 11370–11374; (*d*) X. Feng, C. Qi, H.-T. Feng, Z. Zhao, H. H. Y. Sung, I. D. Williams, R. T. K. Kwok, J. W. Y. Lam, A. Qin and B. Z. Tang, *Chem. Sci.*, 2018, **9**, 5679–5687; (*e*) D. Li, W. Hu, J. Wang, Q. Zhang, X.-M. Cao, X. Ma and H. Tian, *Chem. Sci.*, 2018, **9**, 5709–5715.

4 (*a*) J. Kalinowski, M. Cocchi, D. Virgili, V. Fattori and J. A. G. Williams, *Adv. Mater.*, 2007, **19**, 4000–4005; (*b*) A. Sakai, M. Tanaka, E. Ohta, Y. Yoshimoto, K. Mizuno and H. Ikeda, *Tetrahedron Lett.*, 2012, **53**, 4138–4141; (*c*) Q.-Y. Yang and J.-M. Lehn, *Angew. Chem., Int. Ed.*, 2014, **53**, 4572–4577.

5 (*a*) C.-C. Hsu, C.-C. Lin, P.-T. Chou, C.-H. Lai, C.-W. Hsu, C.-H. Lin and Y. Chi, *J. Am. Chem. Soc.*, 2012, **134**, 7715–7724; (*b*) F. Geist, A. Jackel and R. F. Winter, *Dalton Trans.*, 2015, **44**, 3974–3987; (*c*) Z. Mao, Z. Yang, Y. Mu, Y. Zhang, Y.-F. Wang, Z. Chi, C.-C. Lo, S. Liu, A. Lien and J. Xu, *Angew. Chem., Int. Ed.*, 2015, **54**, 6270–6273; (*d*) P. Irmler and R. F. Winter, *Dalton Trans.*, 2016, **45**, 10420–10434; (*e*) I. Kondrasenko, K.-Y. Chung, Y.-T. Chen, J. Koivistoinen, E. V. Grachova, A. J. Karttunen, P.-T. Chou and I. O. Koshevoy, *J. Phys. Chem. C*, 2016, **120**, 12196–12206; (*f*) H. Wu, C. Hang, X. Li, L. Yin, M. Zhu, J. Zhang, Y. Zhou, H. Ågren, Q. Zhang and L. Zhu, *Chem. Commun.*, 2017, **53**, 2661–2664; (*g*) C. Zhou, S. Zhang, Y. Gao, H. Liu, T. Shan, X. Liang, B. Yang and Y. Ma, *Adv. Funct. Mater.*, 2018, **28**, 1802407; (*h*) K. Tabata, T. Yamada, H. Kita and Y. Yamamoto, *Adv. Funct. Mater.*, 2019, **29**, 1805824.

6 (*a*) R. Kawagoe, I. Takashima, S. Uchinomiya and A. Ojida, *Chem. Sci.*, 2017, **8**, 1134–1140; (*b*) Y. Okorochenkova, M. Porubský, S. Benická and J. Hlaváč, *Chem. Commun.*, 2018, **54**, 7589–7592.

7 (*a*) J. E. Yarnell, J. C. Deaton, C. E. McCusker and F. N. Castellano, *Inorg. Chem.*, 2011, **50**, 7820–7830; (*b*) T. Yoshihara, Y. Yamaguchi, M. Hosaka, T. Takeuchi and S. Tobita, *Angew. Chem., Int. Ed.*, 2012, **51**, 4148–4151; (*c*) Q. Zhao, X. Zhou, T. Cao, K. Y. Zhang, L. Yang, S. Liu, H. Liang, H. Yang, F. Li and W. Huang, *Chem. Sci.*, 2015, **6**, 1825–1831; (*d*) S. K. Gupta, A. Haridas and J. Choudhury, *Chem. – Eur. J.*, 2017, **23**, 4770–4773.

8 (*a*) S. Van Wallendael and D. P. Rillema, *J. Chem. Soc., Chem. Commun.*, 1990, 1081–1082; (*b*) E. C. Glazer, D. Magde and Y. Tor, *J. Am. Chem. Soc.*, 2005, **127**, 4190–4192; (*c*) Z. Chen, K. Y. Zhang, X. Tong, Y. Liu, C. Hu, S. Liu, Q. Yu, Q. Zhao and W. Huang, *Adv. Funct. Mater.*, 2016, **26**, 4386–4396; (*d*) K. S. Kisel, A. S. Melnikov, E. V. Grachova, P. Hirva, S. P. Tunik and I. O. Koshevoy, *Chem. – Eur. J.*, 2017, **23**, 11301–11311; (*e*) Z. Hao, F. Meng, P. Wang, Y. Wang, H. Tan, Y. Pei, S. Su and Y. Liu, *Dalton Trans.*, 2017, **46**, 16257–16268; (*f*) F. Liu, J. Wen, S.-S. Chen and S. Sun, *Chem. Commun.*, 2018, **54**, 1371–1374.

9 (*a*) J.-C. G. Bünzli and C. Piguet, *Chem. Soc. Rev.*, 2005, **34**, 1048–1077; (*b*) M. D. Ward, *Coord. Chem. Rev.*, 2010, **254**, 2634–2642; (*c*) S. V. Eliseeva and J.-C. G. Bünzli, *Chem. Soc. Rev.*, 2010, **39**, 189–227; (*d*) H.-B. Xu, J.-G. Deng and B. Kang, *RSC Adv.*, 2013, **3**, 11367–11384; (*e*) M. Pan, W.-M. Liao, S.-Y. Yin, S.-S. Sun and C.-Y. Su, *Chem. Rev.*, 2018, **118**, 8889–8935.

10 (*a*) T. J. Sørensen, M. Tropiano, O. A. Blackburn, J. A. Tilney, A. M. Kenwright and S. Faulkner, *Chem. Commun.*, 2013, **49**, 783–785; (*b*) T. J. Sørensen, A. M. Kenwright and S. Faulkner, *Chem. Sci.*, 2015, **6**, 2054–2059; (*c*) O. Kotova, S. Comby, C. Lincheneau and T. Gunnlaugsson, *Chem. Sci.*, 2017, **8**, 3419–3426.

11 (*a*) M. Tropiano and S. Faulkner, *Chem. Commun.*, 2014, **50**, 4696–4698; (*b*) S. Shuvaev, M. Starck and D. Parker, *Chem. – Eur. J.*, 2017, **23**, 9974–9989; (*c*) S.-Y. Huang and V. C. Pierre, *Chem. Commun.*, 2018, **54**, 9210–9213; (*d*) G. Bao, S. Zha, Z. Liu, Y.-H. Fung, C.-F. Chan, H. Li, P.-H. Chu, D. Jin, P. A. Tanner and K.-L. Wong, *Inorg. Chem.*, 2018, **57**, 120–128.

12 (*a*) H. Peng, M. I. J. Stich, J. Yu, L.-N. Sun, L. H. Fischer and O. S. Wolfbeis, *Adv. Mater.*, 2010, **22**, 716–719; (*b*) K. Yanagisawa, Y. Kitagawa, T. Nakanishi, T. Seki, K. Fushimi, H. Ito and Y. Hasegawa, *Chem. – Eur. J.*, 2018, **24**, 1956–1961; (*c*) X.-Q. Guo, L.-P. Zhou, L.-X. Cai and Q.-F. Sun, *Chem. – Eur. J.*, 2018, **24**, 6936–6940; (*d*) H. Zhang, J. Jiang, P. Gao, T. Yang, K. Y. Zhang, Z. Chen, S. Liu, W. Huang and Q. Zhao, *ACS Appl. Mater. Interfaces*, 2018, **10**, 17542–17550.

13 (*a*) A. J. Amoroso and S. J. A. Pope, *Chem. Soc. Rev.*, 2015, **44**, 4723–4742; (*b*) J.-C. G. Bünzli, *J. Lumin.*, 2016, **170**, 866–878; (*c*) K. Y. Zhang, Q. Yu, H. Wei, S. Liu, Q. Zhao and W. Huang, *Chem. Rev.*, 2018, **118**, 1770–1839.

14 O. Laporte and W. F. Meggers, *J. Opt. Soc. Am.*, 1925, **11**, 459–463.

15 M. D. Ward, *Coord. Chem. Rev.*, 2007, **251**, 1663–1677.

16 P. Coppo, M. Duati, V. N. Kozhevnikov, J. W. Hofstraat and L. De Cola, *Angew. Chem., Int. Ed.*, 2005, **44**, 1806–1810.

17 (*a*) T. K. Ronson, T. Lazarides, H. Adams, S. J. A. Pope, D. Sykes, S. Faulkner, S. J. Coles, M. B. Hursthouse, W. Clegg, R. W. Harrington and M. D. Ward, *Chem. – Eur. J.*, 2006, **12**, 9299–9313; (*b*) F. Kennedy, N. M. Shavaleev, T. Koullourou, Z. R. Bell, J. C. Jeffery, S. Faulkner and M. D. Ward, *Dalton Trans.*, 2007, 1492–1499; (*c*) H.-B. Xu, J. Ni, K.-J. Chen, L.-Y. Zhang and Z.-N. Chen, *Organometallics*, 2008, **27**, 5665–5671; (*d*) O. J. Stacey, A. J. Amoroso, J. A. Platts, P. N. Horton, S. J. Coles, D. Lloyd, C. F. Williams, A. J. Hayes, J. J. Dunsford and S. J. A. Pope, *Chem. Commun.*, 2015, **51**, 12305–12308.

18 (*a*) D. Sykes, I. S. Tidmarsh, A. Barbieri, I. V. Sazanovich, J. A. Weinstein and M. D. Ward, *Inorg. Chem.*, 2011, **50**, 11323–11339; (*b*) A. Baschieri, S. Muzzioli, E. Matteucci, S. Stagni, M. Massi and L. Sambri, *Dalton Trans.*, 2015, **44**, 37–40; (*c*) A. Jana, B. J. Crowston, J. R. Shewring, L. K. McKenzie, H. E. Bryant, S. W. Botchway, A. D. Ward, A. J. Amoroso, E. Baggaley and M. D. Ward, *Inorg. Chem.*, 2016, **55**, 5623–5633.

19 T. Lazarides, N. M. Tart, D. Sykes, S. Faulkner, A. Barbieri and M. D. Ward, *Dalton Trans.*, 2009, 3971–3979, DOI: 10.1039/B901560D.

20 K. Sénéchal-David, S. J. A. Pope, S. Quinn, S. Faulkner and T. Gunnlaugsson, *Inorg. Chem.*, 2006, **45**, 10040–10042.

21 L. R. Hill, O. A. Blackburn, M. W. Jones, M. Tropiano, T. J. Sørensen and S. Faulkner, *Dalton Trans.*, 2013, **42**, 16255–16258.

22 (*a*) S. J. A. Pope, *Polyhedron*, 2007, **26**, 4818–4824; (*b*) M. Andrews, J. E. Jones, L. P. Harding and S. J. A. Pope, *Chem. Commun.*, 2011, **47**, 206–208.

23 (*a*) J. Wang, H. Chen, F. Ru, Z. Zhang, X. Mao, D. Shan, J. Chen and X. Lu, *Chem. – Eur. J.*, 2018, **24**, 3499–3505; (*b*) M. Rong, X. Yang, L. Huang, S. Chi, Y. Zhou, Y. Shen, B. Chen, X. Deng and Z.-Q. Liu, *ACS Appl. Mater. Interfaces*, 2019, **11**, 2336–2343.

24 G. He, D. Guo, C. He, X. Zhang, X. Zhao and C. Duan, *Angew. Chem., Int. Ed.*, 2009, **48**, 6132–6135.

25 (*a*) G.-L. Law, K.-L. Wong, H.-L. Tam, K.-W. Cheah and W.-T. Wong, *Inorg. Chem.*, 2009, **48**, 10492–10494; (*b*) A. H. Shelton, I. V. Sazanovich, J. A. Weinstein and M. D. Ward, *Chem. Commun.*, 2012, **48**, 2749–2751; (*c*) J. Zhang, H. Li, P. Chen, W. Sun, T. Gao and P. Yan, *J. Mater. Chem. C*, 2015, **3**, 1799–1806; (*d*) K. Singh, R. Boddula and S. Vaidyanathan, *Inorg. Chem.*, 2017, **56**, 9376–9390; (*e*) R. Boddula, K. Singh, S. Giri and S. Vaidyanathan, *Inorg. Chem.*, 2017, **56**, 10127–10130.

26 H.-B. Xu, P.-C. Jiao, B. Kang, J.-G. Deng and Y. Zhang, *Sci. Rep.*, 2013, **3**, 2199.

27 (*a*) P.-A. Bouit, A. Escande, R. Szűcs, D. Szieberth, C. Lescop, L. Nyulászi, M. Hissler and R. Réau, *J. Am. Chem. Soc.*, 2012, **134**, 6524–6527; (*b*) X.-K. Liu, C.-J. Zheng,

M.-F. Lo, J. Xiao, C.-S. Lee, M.-K. Fung and X.-H. Zhang, *Chem. Commun.*, 2014, **50**, 2027–2029; (*c*) E. Yamaguchi, C. Wang, A. Fukazawa, M. Taki, Y. Sato, T. Sasaki, M. Ueda, N. Sasaki, T. Higashiyama and S. Yamaguchi, *Angew. Chem., Int. Ed.*, 2015, **54**, 4539–4543; (*d*) I. Kondrasenko, Z.-H. Tsai, K.-Y. Chung, Y.-T. Chen, Y. Y. Ershova, A. Doménech-Carbó, W.-Y. Hung, P.-T. Chou, A. J. Karttunen and I. O. Koshevoy, *ACS Appl. Mater. Interfaces*, 2016, **8**, 10968–10976.

28 X. Yang, X. Yan, H. Guo, B. Liu, J. Zhao, G. Zhou, Y. Wu, Z. Wu and W.-Y. Wong, *Dyes Pigm.*, 2017, **143**, 151–164.

29 Z. H. Li, M. S. Wong, Y. Tao and M. D'Iorio, *J. Org. Chem.*, 2004, **69**, 921–927.

30 A. Belyaev, Y.-H. Cheng, Z.-Y. Liu, A. J. Karttunen, P.-T. Chou and I. O. Koshevoy, *Angew. Chem., Int. Ed.*, 2019, **58**, 13456–13465.

31 I. V. Solovjov, A. Kondinski, K. Y. Monakhov, I. O. Koshevoy and E. V. Grachova, *Inorg. Chem. Front.*, 2018, **5**, 160–171.

32 (*a*) G. E. Coates and C. Parkin, *J. Chem. Soc.*, 1962, 3220–3226; (*b*) V. W.-W. Yam, S. W.-K. Choi and K.-K. Cheung, *Organometallics*, 1996, **15**, 1734–1739.

33 (*a*) J. P. Perdew, K. Burke and M. Ernzerhof, *Phys. Rev. Lett.*, 1996, **77**, 3865–3868; (*b*) H. Iikura, T. Tsuneda, T. Yanai and K. Hirao, *J. Chem. Phys.*, 2001, **115**, 3540–3544.

34 V. Khistiaeva, A. S. Melnikov, S. Slavova, V. Sizov, G. L. Starova, I. O. Koshevoy and E. V. Grachova, *Inorg. Chem. Front.*, 2018, **5**, 3015–3027.

35 Y.-C. Chang, K.-C. Tang, H.-A. Pan, S.-H. Liu, I. O. Koshevoy, A. J. Karttunen, W.-Y. Hung, M.-H. Cheng and P.-T. Chou, *J. Phys. Chem. C*, 2013, **117**, 9623–9632.

36 W. T. Carnall, G. L. Goodman, K. Rajnak and R. S. Rana, *J. Chem. Phys.*, 1989, **90**, 3443–3457.

37 H. Xu, K. Yin and W. Huang, *ChemPhysChem*, 2008, **9**, 1752–1760.

38 G. Chen, W. Li, T. Zhou, Q. Peng, D. Zhai, H. Li, W. Z. Yuan, Y. Zhang and B. Z. Tang, *Adv. Mater.*, 2015, **27**, 4496–4501.

39 (*a*) M. Maus, W. Rettig, D. Bonafoux and R. Lapouyade, *J. Phys. Chem. A*, 1999, **103**, 3388–3401; (*b*) E. Sakuda, Y. Ando, A. Ito and N. Kitamura, *J. Phys. Chem. A*, 2010, **114**, 9144–9150.